

# Supramolecular Assemblies of a Naturally Derived Sophorolipid

Shuiqin Zhou,<sup>\*,†</sup> Chang Xu,<sup>†</sup> Jun Wang,<sup>†</sup> Wei Gao,<sup>‡</sup> Rena Akhverdiyeva,<sup>‡</sup>  
Vishal Shah,<sup>‡</sup> and Richard Gross<sup>\*,‡</sup>

Department of Chemistry and Institute of Macromolecular Assembly, College of Staten Island,  
The City University of New York, 2800 Victory Boulevard, Staten Island, New York 10314,  
and NSF Center for Biocatalysis and Bioprocessing of Macromolecules,  
Department of Chemistry and Chemical Engineering, Polytechnic University,  
Six Metrotech Center, Brooklyn, New York 11201

Received June 8, 2004

Acidic sophorolipid (SL) molecules derived from yeasts represent a novel type of asymmetrical bolaamphiphiles due to their unique structural features that include an asymmetrical polar head size (disaccharide vs COOH), a kinked hydrophobic core (*cis*-9-octadecenoic chain), and a non-amide polar–nonpolar linkage. Light microscopy, small- and wide-angle X-ray scattering, FT-IR spectroscopy, and dynamic laser light scattering were used to investigate the supramolecular structures of the self-assembled aggregates of SL molecules at different pH values. In acidic conditions (pH < 5.5), giant twisted and helical ribbons of 5–11  $\mu\text{m}$  width and several hundreds of micrometers length were observed for the first time. Increase in solution pH values slowed ribbon formation, decreased ribbon yield, and increased the helicity and entanglements of the giant ribbons. An interdigitated lamellar packing model of acidic SL–COOH molecules with a long period of 2.78 nm, stabilized by both the strong hydrophobic association between the *cis*-9-octadecenoic chains and strong disaccharide–disaccharide hydrogen bonding, is proposed. The neutralization of SL–COOH in water to SL–COONa produced clear solutions with the formation of short-range ordered aggregates. At concentrations below 1.0 mg/mL, the size of self-assembled aggregates increased as the concentration increased. At concentrations above 1.0 mg/mL, narrowly distributed micellar aggregates with a constant hydrodynamic radius ( $R_h$ ) of about 100 nm are formed. The large micelles show strong angular dependence with the fast mode appearing at scattering angle  $\theta \geq 60^\circ$ .

## Introduction

Bolaamphiphiles (“bolas”), bearing polar groups at both ends of a hydrophobe, can complement many of the deficiencies of nonfunctional lipids such as the poor stability as well as the limited structural and chemical versatility of their self-assemblies.<sup>1–5</sup> Bolas tend to form well-defined supramolecular structures under mild conditions and have high biological relevance as mimics of natural transmembrane lipids.<sup>6,7</sup> Numerous symmetrical bolas bearing phosphatidyls,<sup>8–13</sup> amino acids,<sup>14,15</sup> monosaccharides,<sup>16–21</sup> urocanic acid,<sup>22</sup> and nucleotides<sup>23</sup> as head-

groups and linear methylene chains or diacetylene chains as the hydrophobic middle block have been synthesized and investigated. Supramolecular structures of monolayer vesicles, helical fibers, helical ribbons, nanotubules, and rigid rods have been observed.<sup>4,14,21–26</sup> Asymmetrical bolas bearing two different polar heads at opposite ends of the lipophilic core have greater structural and chemical versatility. Thus, they are expected to bring unique structural and physicochemical properties as well as

\* To whom correspondence should be addressed. E-mail: zhoush@mail.csi.cuny.edu; rgross@duke.poly.edu.

<sup>†</sup> College of Staten Island, City University of New York.

<sup>‡</sup> Polytechnic University.

(1) Fuhrhop, J. H.; Fritsch, D. *Acc. Chem. Res.* **1986**, *19*, 130–137.  
(2) Fyles, T. M.; Looock, D.; Zhou, X. *J. Am. Chem. Soc.* **1998**, *120*, 2997–3003.

(3) Moss, R. A.; Li, G.; Li, J. M. *J. Am. Chem. Soc.* **1994**, *116*, 805–806.

(4) Meglio, C. D.; Rananavare, S. B.; Svenson, S.; Thompson, D. H. *Langmuir* **2000**, *16*, 128–133.

(5) Song, J.; Cheng, Q.; Kopta, S.; Stevens, R. C. *J. Am. Chem. Soc.* **2001**, *123*, 3205–3213.

(6) De Rosa, R.; Morana, A. In *Neural Networks and Biomolecular Engineering to Bioelectronics*; Nicolini, N., Ed.; Plenum Press: New York, 1995; p 217.

(7) Lee, J.; Jung, S.; Lowe, S.; Zeikus, J. G.; Hollingsworth, R. I. *J. Am. Chem. Soc.* **1998**, *120*, 5855–5863.

(8) Kim, J. M.; Thomposon, D. H. *Langmuir* **1992**, *8*, 637–644.

(9) Menger, F. M.; Chen, X. Y.; Brocchini, S.; Hopkins, H. P.; Hamilton, D. *J. Am. Chem. Soc.* **1993**, *115*, 6600–6608.

(10) Thompson, D. H.; Svendsen, C. B.; Di Meglio, C.; Anderson, V. C. *J. Org. Chem.* **1994**, *59*, 2945–2955.

(11) Svenson, S.; Thompson, D. H. *J. Org. Chem.* **1998**, *63*, 7180–7182.

(12) Arakawa, K.; Eguchi, T.; Kakinuma, K. *J. Org. Chem.* **1998**, *63*, 4741–4745.

(13) Wang, G.; Hollingsworth, R. I. *J. Org. Chem.* **1999**, *64*, 4140–4147.

(14) Kogiso, M.; Ohnishi, S.; Yase, K.; Masuda, M.; Shimizu, T. *Langmuir* **1998**, *14*, 4978–4986.

(15) Schneider, J.; Messerschmidt, C.; Schultz, A.; Gnada, M.; Schade, B.; Luger, P.; Bombicz, P.; Hubert, V.; Fuhrhop, J. H. *Langmuir* **2000**, *16*, 8575–8584.

(16) Andre, D.; Luger, P.; Nehmzow, D.; Fuhrhop, J. H. *Carbohydr. Res.* **1994**, *261*, 1–11.

(17) Goueth, P.; Ramiz, A.; Ronco, G.; Mackenzie, G.; Villa, P. *Carbohydr. Res.* **1994**, *266*, 171–189.

(18) Bertho, J. N.; Coue, A.; Ewing, D. F.; Goodby, J. W.; Letellier, P.; Mackenzie, G.; Plusquellec, D. *Carbohydr. Res.* **1997**, *300*, 341–346.

(19) Shimizu, T.; Masuda, M. *J. Am. Chem. Soc.* **1997**, *119*, 2812–2818.

(20) Pestman, J. M.; Terpstra, K. R.; Stuart, M. C. A.; Van Doren, H. A.; Brisson, A.; Kellogg, R. M.; Engberts, J. B. F. N. *Langmuir* **1997**, *13*, 6857–6860.

(21) Masuda, M.; Hanada, T.; Okada, Y.; Yase, K.; Shimizu, T. *Macromolecules* **2000**, *33*, 9233–9238.

(22) Sirieix, J.; Viguier, N. L.; Riviere, M.; Lattes, A. *Langmuir* **2000**, *16*, 9221–9224.

(23) Iwaura, R.; Yoshida, K.; Masuda, M.; Yase, K.; Shimizu, T. *Chem. Mater.* **2002**, *14*, 3047–3053.

(24) Nakazawa, I.; Masuda, M.; Okada, Y.; Hanada, T.; Yase, K.; Asai, M.; Shimizu, T. *Langmuir* **1999**, *15*, 4757–4764.

(25) Matsui, H.; Gologan, B. *J. Phys. Chem. B* **2000**, *104*, 3383–3386.

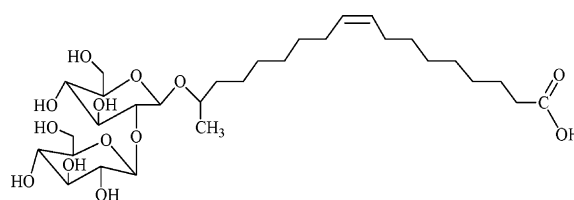
(26) Shimizu, T.; Iwaura, R.; Masuda, M.; Hanada, T.; Yase, K. *J. Am. Chem. Soc.* **2001**, *123*, 5947–5955.

functionality to self-assembled materials. However, despite the increasing number of studies on symmetrical synthetic bolas, few studies have been carried on asymmetrical bolas. This is likely because, relative to symmetrical bolas, asymmetrical bolas generally require more complex syntheses with multiple protection–deprotection steps.<sup>5,15,27–29</sup>

Fuhrhop and co-workers<sup>15,27,30</sup> did pioneering work on the self-assembly of asymmetrical bolas. They reported that bolaform amphiphiles with a rigid hydrophobic bixin core and gluconamide and methyl ester as respective end groups could be effectively integrated into helical micellar fibers.<sup>30</sup> They also studied molecules with polar headgroups that were either two different amino acids or one amino acid and an amine linked by oligomethylene spacers.<sup>15,17</sup> Structures of monolayer nanorods and tubules, crystals, flat ribbons of about 1  $\mu\text{m}$  width, and helical and straight fibers were observed. The self-assembled structures depended on whether the oligomethylene spacer had an odd or even number of carbons due to the dominant effect of intermolecular diamide hydrogen bonding. The self-assembly of bolas consisting of diacetylene containing a hydrophobic spacer, an amide-linked glutamic acid as one polar head, and a carboxylic acid as the other produced flat ribbons with widths of 0.2–0.5  $\mu\text{m}$  in water.<sup>5</sup> Narrower helical ribbons were formed by the rupture of these flat ribbons. Guilbot et al.<sup>29</sup> synthesized another type of asymmetrical bola with glycosidic and cationic trimethylene ammonium headgroups linked by a diamide oligomethylene spacer. Monolayer vesicles were observed in water. Although the fundamentals of structure formation by asymmetrical bolas remain to be elucidated, it appears that molecular chirality, hydrogen-bonding sites, charges, steric interactions between polar heads, the nature of hydrophobic associations, and the building of  $\pi$ – $\pi$  stacking within the hydrophobic spacer are critical factors that govern the formation of supramolecular structures. In many cases, the development of intermolecular hydrogen bonding between amide groups at polar–nonpolar linkage sites played an important role in the generation of long-range ordered assemblies.

In this paper, we report the pH-dependent supramolecular assembly of an acidic sophorolipid (SL). Acidic SL is one component of a mixture of glycolipid biosurfactants that are produced by culturing the yeast *Candida bombicola* on mixtures of carbohydrates and lipids.<sup>31</sup> These glycolipids have great potential as therapeutics for the treatment of cancer and severe immune disorders<sup>32,33</sup> and in enhanced oil recovery,<sup>34</sup> germicidal preparations,<sup>35</sup> and cosmetics.<sup>36</sup> The natural mixture of sophorolipids produced by the yeast was chemically converted to form an acidic SL product (SL–COOH, see Chart 1).<sup>37</sup> The complex and

Chart 1. Chemical Structure of the Acidic SL Molecule



unique structure of SL–COOH, molecularly engineered by nature, provides an intriguing asymmetric bola for study of its self-assembly characteristics. Unique features of SL–COOH include a large differential in size between the sophorose and carboxylic acid polar headgroups. Furthermore, the disaccharide polar head with seven hydroxyl groups and four ether oxygen atoms provides many sites for intermolecular association via hydrogen bonding. Third, unlike the linear configuration of methylene or *trans*-diacetylene chains of previously studied asymmetric bolas, the middle hydrophobic core of *cis*-9-octadecenoic chains has a kinked wedge-shape configuration with equal carbon numbers at both sides of the monounsaturated double bond. Moreover, the SL–COOH molecules lack amide bonds between the polar head and hydrophobic core that often control the molecular packing of asymmetric bolas. These unique molecular features of acidic SLs lead to novel supramolecular structures and morphologies that allow us to build on our limited knowledge of how structural properties of asymmetric bolas confer specific supermolecular structures from self-assembled systems.

## Experimental Section

**Materials.** The media chemicals (glucose, urea, and oleic acids) for fermentation were obtained from Aldrich Co. All chemicals and solvents used for this investigation were analytical grade and were used as received unless otherwise noted. The water used for sample preparation was purified through a Millipore Milli-Q system with a resistivity of 18.2 M $\Omega$  cm.

**Synthesis and Isolation of Acidic SL.** A sophorolipid mixture was synthesized by fermentation of *C. bombicola*.<sup>37</sup> The fermentation medium was composed of glucose (100 g), yeast extract (10 g), urea (1 g), and oleic acid (40 g) in 1000 mL of water. After 7 days of fermentation, sophorolipid was extracted thrice using ethyl acetate. The extracts were pooled, and the solvent then was removed. The obtained product was therein washed with hexane to remove the residual fatty acids. Acidic sophorolipids were synthesized from these natural mixtures through alkaline hydrolysis following a procedure described in the literature.<sup>38</sup> The hydrolyzed sophorolipid mixture was acidified, instead of extraction with *n*-pentanol, the solution was cooled in an ice bath, and the precipitate was further purified by silica gel column chromatography using a gradient solvent system of chloroform/methanol (3:22 to 4:22, v/v). The product was identified by NMR<sup>38</sup> and liquid chromatography–mass spectrometry.<sup>39</sup>

**Preparation and Observation of Supramolecular Ribbons.** The acidic SL molecules rapidly dissolve at room temperature in deionized water at concentrations between 1.0 and 5.0 mg/mL to give clear solutions. A freshly prepared SL–COOH aqueous solution at 2.0 mg/mL had a pH value of 5.05. Dilute HCl or NaOH solutions were used to adjust the pH of solutions to the desired value. At acidic pH values (pH < 5.5) and room temperature, solidlike supramolecular aggregates slowly form. The kinetics of the microstructure formation depends on the initial pH value. To view the microstructures of the solidlike aggregates, a drop of the dispersion containing the self-assembled

(27) Fuhrhop, J. H.; Spiroski, D.; Boettcher, C. *J. Am. Chem. Soc.* **1993**, *115*, 1600–1601.

(28) Lecollinet, G.; Auzley-Velty, R.; Danel, M.; Benvegna, T.; Mackenzie, G.; Goodby, J. W.; Plusquellec, D. *J. Org. Chem.* **1999**, *64*, 3139–3150.

(29) Guilbot, J.; Benvegna, T.; Legros, N.; Plusquellec, D. *Langmuir* **2001**, *17*, 613–618.

(30) Fuhrhop, J. H.; Krull, M.; Schulz, A.; Mobius, D. *Langmuir* **1990**, *6*, 497–505.

(31) Asmer, H. J.; Lang, S.; Wagner, F.; Wray, V. H. *J. Am. Oil Chem. Soc.* **1988**, *65*, 1460–1466.

(32) Isoda, H.; Kitamoto, D.; Shinmoto, H.; Matsumura, M.; Nakahara, T. *Biosci. Biotechnol. Biochem.* **1997**, *61*, 609–614.

(33) Piljac, G.; Piljac, V. U.S. Patent 5,514,661, 1996; U.S. Patent 5,455,232, 1995.

(34) McInerney, M. J.; Jenneman, G. E.; Knapp, R. M.; Menzie, D. U.S. Patent 4,522,261, 1995.

(35) Pierce, D.; Heilman, T. J. World Patent 9,816,192, 1998.

(36) Maingault, M. U.S. Patent 5,981,497, 1999.

(37) Bisht, K. S.; Gross, R. A.; Kaplan, D. *J. Org. Chem.* **1999**, *64*, 780–789.

(38) Rau, U.; Heckmann, R.; Wray, V.; Lang, S. *Biotechnol. Lett.* **1999**, *21*, 973–977.

(39) Nunez, A.; Ashby, R.; Foglia, T. A.; Solaiamn, D. K. Y. *Chromatographia* **2001**, *53*, 673–677.

materials was placed on a glass slide and covered with a coverslip. The samples were examined by using a Nikon Labophot-2-pol light microscope with 10 $\times$ , 20 $\times$ , 40 $\times$ , and 100 $\times$  objectives. The micrograph images were recorded by a highly sensitive camera (Olympus SC35 type 12), processed on photographic paper, and scanned to the computer.

**X-ray Scattering Measurements.** The solidlike aggregated ribbon samples, either equilibrated with the aqueous solution in which they were initially formed or completely dried, were directly placed into the sample holder. Small-angle X-ray scattering (SAXS) and wide-angle X-ray scattering (WAXS) measurements were carried out at the SUNY X3A2 beamline at the National Synchrotron Light Source (NSLS), Brookhaven National Laboratory (BNL). A laser-aided prealigned pinhole collimator was used to define the incident X-ray beam. The incident X-ray wavelength ( $\lambda$ ) was tuned at 0.1542 nm. A two-dimensional imaging plate was used in conjunction with an image scanner as the detection system.<sup>40,41</sup> The sample to detector distance for SAXS was 841.9 mm. For WAXS, the sample–detector distance, calibrated using an Al<sub>2</sub>O<sub>3</sub> standard, was 100.0 mm. The scattering vector  $q$  is expressed as  $q = (4\pi/\lambda) \sin(\theta/2)$  with  $\theta$  being the scattering angle between the incident and the scattered X-rays. The  $d$  spacing of the ordered structures was calculated as  $d = 2\pi/q$ .

**Dynamic Laser Light Scattering (LLS) Measurements.** A standard LLS spectrometer (BI-200SM) equipped with a BI-9000 AT digital time correlator (Brookhaven Instrument Inc.) and a solid-state laser (DPSS, SUWTECH, 200 mW, 532 nm) was used to perform LLS studies over a scattering angular range of  $\theta = 15$ –150°. The temperature was controlled at  $25 \pm 0.1$  °C. Freshly prepared SL solutions were passed through a 0.45  $\mu\text{m}$  Millipore Millex-HN filter to remove dust before LLS measurements. The Laplace inversion of each measured intensity–intensity time correlated function in a dilute solution can result in a characteristic line width distribution  $G(\Gamma)$ . For a purely diffusive relaxation,  $\Gamma$  is related to the translational diffusion coefficient  $D$  by  $(\Gamma/q^2)_{C \rightarrow 0, q \rightarrow 0} = D$ , where  $q = (4\pi n/\lambda) \sin(\theta/2)$  with  $n$ ,  $\lambda$ , and  $\theta$  being the solvent refractive index, the wavelength of the incident light in vacuo, and the scattering angle, respectively.  $G(\Gamma)$  can be further converted to a hydrodynamic radius distribution by using the Stokes–Einstein equation,  $R_h = (k_B T / 6\pi\eta) D^{-1}$ , where  $T$ ,  $k_B$ , and  $\eta$  are the absolute temperature, the Boltzmann constant, and the solvent viscosity, respectively.<sup>42,43</sup>

**Fourier Transform Infrared (IR) Spectroscopy.** The solidlike ribbons formed from the self-assembly of SL–COOH molecules or the dispersions of micellar aggregates from the self-assembly of SL–COONa molecules were mixed with IR-grade KBr, dried in a vacuum oven, and ground up, and pellets were pressed for IR measurements. The IR spectra were collected using a Fourier transform spectrometer (Nicolet Magna 550) operating at a 2  $\text{cm}^{-1}$  resolution.

## Results and Discussion

**Formation of Solidlike Giant Ribbons.** Solidlike giant ribbons from the self-assembly of acidic SL molecules form readily at room temperature. For a fixed initial concentration of acidic SL, the kinetics of ribbon formation and yield of solidlike ribbon products was a function of the initial pH of freshly made solutions. To view ribbon formation, a few drops of freshly made clear SL–COOH solution were placed onto a glass slide and then covered. Figure 1 shows light microscope photographs that document ribbon formation at  $C = 2.0$  mg/mL and  $\text{pH} = 2.0$ .

Initially, both the size and number density of the self-assembled ribbon aggregates were small so that ribbon

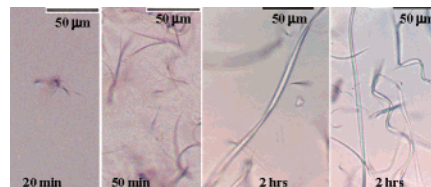


**Figure 1.** Kinetics of giant ribbon formation of SL–COOH at  $\text{pH} = 2.0$ ,  $C = 2.0$  mg/mL, and room temperature monitored by light microscopy.

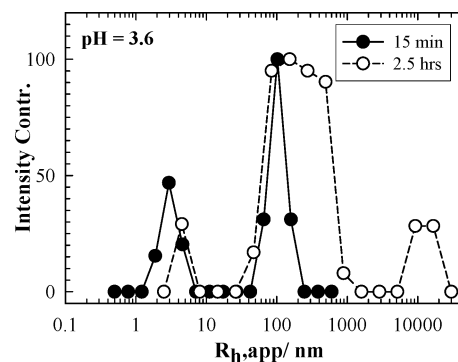


**Figure 2.** Growing kinetics of the self-assembled aggregates of SL–COOH molecules at  $\text{pH} = 3.6$ ,  $C = 2.0$  mg/mL, and  $T = 25$  °C, in terms of  $R_h$  distributions measured by dynamic LLS at  $\theta = 30^\circ$ .

pieces diffused quickly in solution. Their rapid diffusion made it difficult to document this stage by a clear photograph. After 20 min, a number of flowerlike supramolecular aggregates of size 30–50  $\mu\text{m}$  were observed that have small pieces of bended ribbons extending in all directions (Figure 1). The length and the width of the ribbons continued to grow with time. After 50 min, increasing quantities of twisted ribbons or little treelike ribbon pieces with branches were observed. By 2 h, very large twisted ribbons with lengths of a few hundred micrometers and a width of  $\sim 5$   $\mu\text{m}$  had formed. Thus, at low pH, large twisted ribbons are rapidly formed.

By increasing the pH of SL aqueous solutions to 3.6, ribbon formation slowed. Figure 2 depicts the growth of self-assembled aggregates in terms of apparent hydrodynamic radius,  $R_h$ . The dynamic LLS measurements were carried out at a SL concentration of 2.0 mg/mL,  $\text{pH} = 3.6$ ,  $T = 25$  °C, and a scattering angle  $\theta = 30^\circ$ . Once the solution of the acidic SL sample was prepared and filtered to remove the dust particles, the sample was placed into the LLS instrument. Fifteen minutes after the solution was made, two peaks of  $R_h = 2.95$  and 102 nm with an intensity ratio of 1 to 2 were observed. The  $R_h$  of the small species is close to the unimolecular length of the acidic SL, suggesting that the initial aggregates could be small micelles with hydrophobic chains packed into the core and the hydrophilic disaccharide headgroups forming the outer shell. After 2½ h, large aggregates were produced with sizes varying from tens of nanometers to tens of micrometers. Five hours after sample preparation, further association occurs to form precipitates. That is, after 5 h, visible suspended particles were observed in the solution.

Figure 3 shows typical light microscope images of the water-equilibrated solidlike ribbons formed by self-assembly of acidic SLs at pH 3.6. Bulky core–shell ribbon aggregates (A) from the strong association and entanglement of the giant twisted ribbons, individual helical ribbons (B), and helical–flat–helical ribbons (C) were found. In addition, the rupture of the wide ribbons produced narrower ribbon strips ( $\sim 2$ –4  $\mu\text{m}$ ), which

(40) Zhou, S.; Hu, H.; Burger, C.; Chu, B. *Macromolecules* **2001**, *34*, 1772–1778.

(41) Zhou, S.; Yeh, F.; Burger, C.; Chu, B. *J. Phys. Chem. B* **1999**, *103*, 2107–2112.

(42) Chu, B. *Laser Light Scattering: Basic Principles and Practice*, 2nd ed.; Academic Press: New York, 1991.

(43) Zhou, S.; Burger, C.; Chu, B.; Sawamura, M.; Nagahama, N.; Toganoh, M.; Hackler, U. E.; Isobe, H.; Nakamura, E. *Science* **2001**, *291*, 1944–1947.

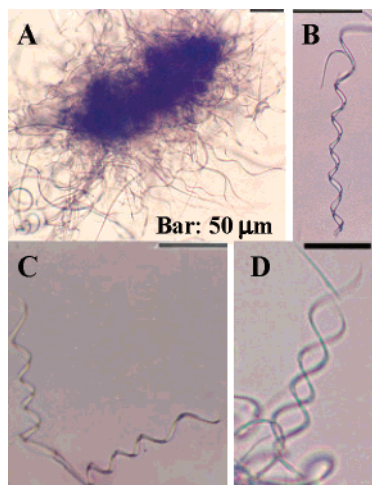


**Figure 3.** Light microscope images of giant ribbons in different morphologies formed by the self-assembly of SL-COOH molecules at pH = 3.6 and room temperature.

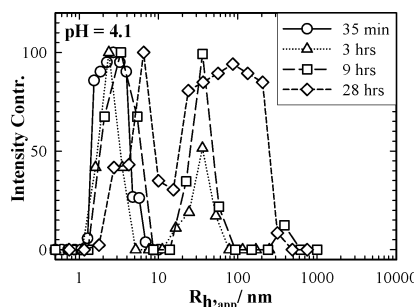


**Figure 4.** Growing kinetics of the self-assembled aggregates of SL-COOH molecules at pH = 4.1,  $C = 2.0$  mg/mL, and  $T = 25$  °C, in terms of  $R_h$  distributions from dynamic LLS measurements at  $\theta = 30^\circ$ .

appeared very flexible so that they formed different entanglements, including double helix (D). In comparison with the slightly twisted ribbons formed at pH = 2.0, the slow formation of ribbons at pH = 3.6 increased the helicity and inter-ribbon entanglements.

When the pH of the freshly made acidic SL solution was adjusted to 4.1, the self-association of the acidic SL molecules slowed dramatically relative to pH 2.0 and 3.6. Figure 4 shows the time dependence of the  $R_h$  distribution for self-assembled particles determined at pH 4.1,  $C = 2.0$  mg/mL,  $T = 25$  °C, and  $\theta = 30^\circ$ . Thirty-five minutes after the solution was made, only one species that corresponds to small micelles with  $\langle R_h \rangle = 2.80$  nm was found. After equilibration for 3 h, a second species with  $R_h \sim 35$  nm had formed. The intensity contribution ratio of the 2.80 and  $\sim 35$  nm species was 2 to 1. That is, the small micelles were still the dominant species in the solution. Extending the equilibration time to 9 h resulted in an increase in the weight fraction of the second species of  $R_h \sim 35$  nm. In addition, a small amount of large aggregates with  $R_h \sim 400$  nm were found. The slow growth continued so that, after 20 h, the aggregates at pH = 4.1 produced visible solidlike particles. By 28 h, a small fraction of the acidic SL molecules self-assembled into solidlike ribbon particles precipitated out. The dynamic LLS measurements for the clear solution in the upper layer showed that the large aggregates in submicron scale with a broad size distribution coexisted with small micelles.

In addition to the strong dependence between ribbon formation and solution pH as described above, the yields of the solidlike ribbon aggregates also decreased sharply

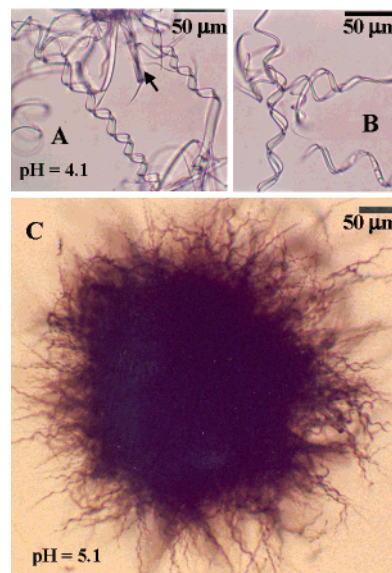


**Figure 5.** Light microscope images of giant ribbons and inter-ribbon entanglements formed by the self-assembly of SL-COOH molecules at room temperature; pH = 4.1 and 5.1, respectively.

with increasing pH. At a fixed initial SL concentration of 2.0 mg/mL, the volume percent of ribbon particles that could be precipitated at pH 1–2 and 4 was about 30 and 10%, respectively. When the initial solution pH was adjusted to 5.9 with dilute NaOH, the clear solution was stable without the formation of solidlike ribbons even after a couple of months. These results suggest that the solidlike ribbon materials are produced from the self-assembly of un-ionized SL-COOH molecules. An increase in the solution pH will result in an increase in the ratio of ionized SL-COO<sup>-</sup> to un-ionized SL-COOH molecules. The charge of the ionized SL-COO<sup>-</sup> molecules can stabilize the initially self-assembled small micelles or ribbon precursors, thus increasing the total number of dispersible aggregates that could be stable in aqueous solution, resulting in low yield of the solidlike ribbon materials.

As mentioned above, the slower growth of ribbons at pH 3.6 relative to 2.0 resulted in an increased helicity of ribbons as well as inter-ribbon entanglements. This pH-induced morphology change of ribbons was also observed for ribbon formation at pH values of 4.1 and 5.1 (Figure 5). At pH = 4.1, the visible solidlike ribbon particles require about 20 h to form. Giant ribbons of hundreds of micrometers long and  $\sim 10$ – $12$   $\mu\text{m}$  wide, packed into parallel strips, were formed either flat or twisted with various degrees of right-handed helicity (Figure 5A,B). A large bundle of parallel ribbon strips could even pack together to form a rod with a diameter of  $\sim 11$   $\mu\text{m}$  (indicated with an arrow in image A). In addition to these individual giant ribbons, very large core-shell ribbon aggregates similar to those in Figure 3C but with higher helicity of extended ribbons were also formed at pH 4.1. Dissolving the SL-COOH molecules into deionized water at 2.0 mg/mL resulted in a clear solution with pH = 5.1. One-week incubation of this solution was required before visible solidlike ribbons were observed. The slow self-assembly of SL-COOH molecules at pH = 5.1 resulted in giant core-shell ribbon aggregates. A typical example of these aggregates is shown in Figure 5C after equilibration of the solution for a week. They consist of a highly dense core surrounded by helical ribbons extending in all directions. In contrast to studies at lower pH values, individual ribbons were rarely found at pH = 5.1.

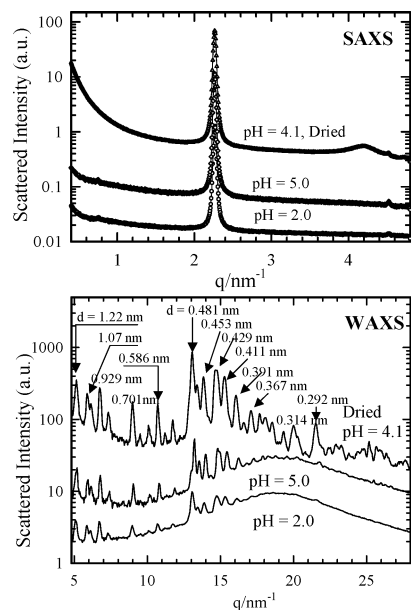


**Figure 6.** SAXS and WAXS patterns of giant SL-COOH ribbons equilibrated in aqueous solutions at pH = 2.0 and 5.0 as well as the dried solid ribbons formed at pH = 4.1, respectively.

**Internal Structures of the Solidlike Giant Ribbons.** To determine how the SL-COOH molecules organize to form giant ribbons, synchrotron SAXS and WAXS measurements were carried out for ribbons formed at different pH values. Figure 6 shows the SAXS and WAXS patterns for ribbons equilibrated in aqueous solutions at pH = 2.0 and 5.0, as well as the dried solid ribbons formed at pH = 4.1. In the SAXS region, all the diffractograms show a sharp intense peak at  $q = 2.26 \text{ nm}^{-1}$  and a weak peak at  $q = 4.52 \text{ nm}^{-1}$  with a spacing ratio of 1:2, indicating that a layered structure with a long period of 2.78 nm ( $d = 2\pi/q_{\text{max}}$ ) was formed. In the dried sample, a broad peak was observed with an interdomain distance of about 1.5 nm. A possible explanation for this peak is that it is from the close packing of small micelles that are stable and diffusive in aqueous solutions (see Figure 4). After drying the samples, these broadly distributed micellar particles might condense together to form a closely packed structure. Nevertheless, regardless of whether the ribbons were dried or equilibrated in aqueous solutions at different pH values, the position of peaks due to the long-range layered structure remained unchanged. This suggests an anhydrous packing of SL-COOH molecules inside the ribbons. In the WAXS region, all of the WAXS diffractograms showed sharp scattering peaks in the  $d$ -space range of 0.37–1.22 nm, which indicates high crystallinity of the hydrocarbon chains and the disaccharide headgroups inside the ribbons. Acidic SL molecules consist of a 17-hydroxyloleic acid chain linked by an acetal bond to the disaccharide sophorose. The distinct difference between the acidic SL molecules and the oleic acid molecules is the disaccharide sophorose head at the end of the methyl-side hydrocarbon chain. Interestingly, oleic acid molecules show only an isotropic phase at temperatures above 12 °C. Below this temperature, crystal structures of the  $\gamma$  or  $\alpha$  phases of a bilayer lamellar packing that have a long period of 4.14 and 4.07 nm, respectively, are formed. In this bilayer packing model, the carboxylic acid groups exist as hydrogen-bond-

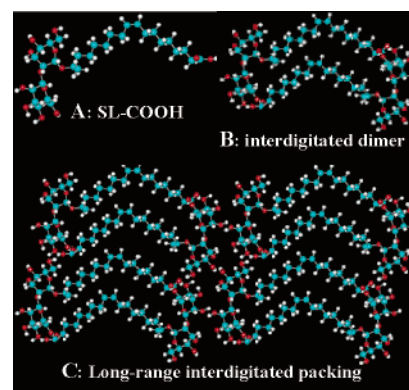


**Figure 7.** Molecular modeling of SL-COOH molecules (A) and a possible interdigitated lamellar packing model of SL-COOH molecules in the giant ribbons (C).

stabilized dimers.<sup>44</sup> In contrast, the acidic SL molecules form highly crystallized lamellar structures at room temperature but with a much shorter long period of 2.78 nm. This lamellar spacing excludes the possibility that a similar bilayer molecular packing was formed in which the acidic SL carboxylic acid groups form hydrogen-bond-stabilized dimers.

Figure 7A shows the molecular modeling of the acidic SL molecule. In this model, the sophorose headgroup is tilted at about 22° relative to the methyl-side hydrocarbon chain. Based on this molecular model, layered structures with a long period of 2.78 nm within the giant ribbons must be formed by interdigitated packing. This ordered structure has the carboxylic acid group of one SL molecule packed closely with the sophorose group of another SL molecule through hydrogen-bonding interactions (Figure 7B). In addition, the hydrocarbon chains are parallel and closely packed. The strong hydrogen bonding between the intermolecular disaccharide headgroups and the strong hydrophobic interactions between the closely packed hydrocarbon chains extended the layered structure to long range. Figure 7C shows a model that depicts how the acidic SL molecules pack together in an interdigitated arrangement to form the highly ordered long-range lamellar structure. This model fits with the experimentally determined long period spacing of 2.78 nm and also requires that the hydrocarbon chains pack as close as possible so that they are highly crystalline. The sharp scattering peaks observed in the WAXS region of Figure 6 also support this model. Generally, the strong reflections in the  $d$ -range of 0.35–0.50 nm could be attributed to the subcell packing of hydrocarbon chains. In terms of the short spacing ratio as well as the relative peak intensity, the peaks at  $d = 0.481$ , 0.453, and 0.429 nm are in agreement with the triclinic parallel subcell ( $T_{\parallel}$ ) observed in the interdigitated  $\beta$  phase of oleic acid,<sup>45</sup> while the peaks at  $d = 0.411$ , 0.391, and 0.367 nm match the orthorhombic parallel ( $O'_{\parallel}$ ) subcell for the carboxyl-side chain packing in the  $\alpha$  and  $\gamma$  phases of oleic acid.<sup>44</sup> These results indicate that two different subcells might coexist for the two differently oriented hydrocarbon chains around the monounsaturated *cis*-C=C bond. Peaks at  $d = 0.929$ , 0.701, and 0.560 nm could be attributed to the higher orders (3rd, 4th, and 5th) of the main lamellar structure with the long period of 2.78 nm. Other major peaks in the WAXS diffractogram at  $d = 1.22$ , 1.07, 0.586, and 0.292 nm fit the layered hydrogen

(44) Tandon, P.; Forster, G.; Neubert, R.; Wartewig, S. *J. Mol. Struct.* **2000**, *524*, 201–215.

(45) Kaneko, F.; Yamazaki, K.; Kitagawa, K.; Kikyo, T.; Kobayashi, M.; Kitagawa, Y.; Matsuura, Y.; Sato, K.; Suzuki, M. *J. Phys. Chem. B* **1997**, *101*, 1803–1809.

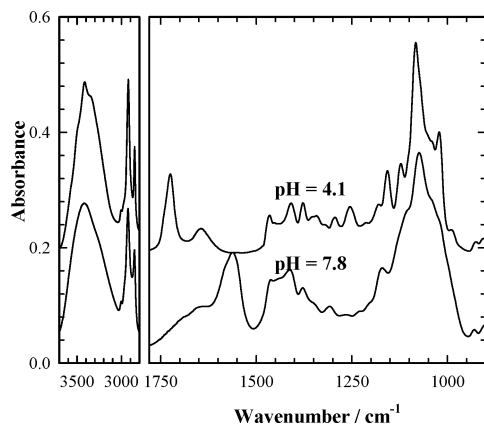


**Figure 8.** FT-IR spectra of the self-assembled ribbons of SL-COOH molecules formed at pH = 4.1 and the soluble micellar aggregates of SL-COONa molecules formed at pH = 7.8, respectively.

bonding of the sophorose headgroups. An important requirement for formation of the unique interdigitated packing model shown in Figure 7B is that the two hydrocarbon chains around the *cis*-C=C bond have a very similar chain length. It is known that the number of carbon atoms between the methyl and carboxyl terminal groups of natural *cis*-monounsaturated fatty acids is an important determinant for the formation of an interdigitated structure.<sup>45</sup> For SL-COOH, critical factors that lead to the close packing of the acidic SL molecules in an interdigitated arrangement are that (i) the two hydrocarbon chains between the mono *cis*-C=C bond and the methyl and carboxyl terminal groups, respectively, have the same length and (ii) the large disparity in size between the relatively small carboxyl and large disaccharide headgroups of this asymmetric bolaamphiphile is suitably accommodated. When the end COOH group of the acidic SL molecules was linked through an amide bond to glutamic acid, there was no observed formation of long-range ordered structures. This occurs regardless of the fact that conjugation of glutamate at the SL carboxyl terminus leads to an end group with an additional carboxyl group to interact through hydrogen bonding with sites of the disaccharide residue and supports the importance of the small size of the SL-COOH carboxyl terminus. Detailed work on the synthesis and physical characterization of SLs conjugated to amino acids will be published separately.

Figure 8 shows FT-IR spectra of the self-assembled ribbons and micellar aggregates formed at pH 4.1 and 7.8, respectively. Clearly, the giant ribbons formed at pH 4.1 that have strong hydrogen bonding between the disaccharide headgroups and highly organized closely packed hydrocarbon chains produced sharper IR bands relative to the short-range ordered micellar aggregates dispersed in aqueous solution at pH 7.8. Prominent differences were observed in a few regions. First, in the carbonyl region of self-assembled ribbons formed at pH 4.1, there is a sharp band at 1725 cm<sup>-1</sup> due to C=O stretching of the carboxyl groups. This band differs from that observed at 1692 cm<sup>-1</sup> for the COOH dimer formed in the  $\gamma$  or  $\alpha$  phases of self-assembled oleic acids.<sup>46</sup> The high frequency of C=O stretching indicates that hydrogen bonding between the carboxylic acid and the hydroxyl groups of neighboring sophorose within the interdigitated structure is relatively weaker than that between carboxylic

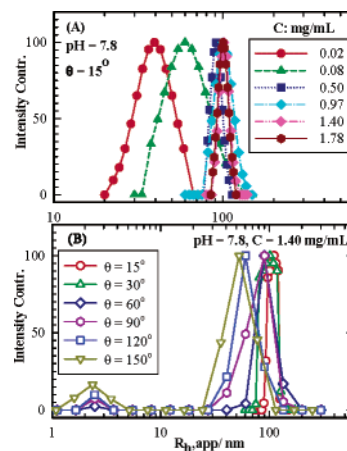


**Figure 9.** (A) Concentration dependence of the  $R_h$  distributions of SL-COONa micellar aggregates formed at pH = 7.8 determined at  $\theta = 15^\circ$ . (B) Angular dependence of the  $R_h$  distributions of SL-COONa micellar aggregates formed at pH = 7.8 and  $C = 1.40$  mg/mL in a  $\theta$  range of 15–150°.

acid dimers within self-assembled oleic acids. In place of the sharp band at 1725 cm<sup>-1</sup>, the micellar aggregates formed at pH 7.8 have a broad band at 1562 cm<sup>-1</sup> characteristic of asymmetric stretching of carboxylate ions (CO<sub>2</sub><sup>-</sup>). Second, in the region from 1000 to 1200 cm<sup>-1</sup>, the FT-IR spectrum of the self-assembled ribbons formed at pH 4.1 showed a series of absorption bands with sharp peaks at 1021 cm<sup>-1</sup> for  $\delta$ (C-OH), 1083 cm<sup>-1</sup> for  $\nu$ (C-O)<sub>exo</sub>, 1122 cm<sup>-1</sup> for  $\nu$ (C-C)/ $\delta$ (C-OH), and 1158 cm<sup>-1</sup> for  $\nu$ (C-OC)/ $\nu$ (C-OH). These sharp peaks merge for the short-range ordered micellar aggregates to form a broad band. Third, a group of C-H and C=C vibrational bands observed for ribbons formed at pH 4.1 disappear or are broadened in the FT-IR spectrum of the micellar aggregates. That is, the band at 1254 cm<sup>-1</sup> for  $\delta$ (C-H) and 1296 cm<sup>-1</sup> for  $\delta$ (CH<sub>2</sub>) disappeared, while the bands at 1340 cm<sup>-1</sup> for  $\rho$ (CH<sub>2</sub>), 1378 cm<sup>-1</sup> for  $\omega$ (CH<sub>2</sub>)/ $\delta_s$ (CH<sub>3</sub>), 1409 cm<sup>-1</sup> for  $\delta_{as}$ (CH<sub>3</sub>)/ $\delta$ (CH), and 1465 cm<sup>-1</sup> for  $\delta$ (CH<sub>2</sub>) merged to form a broad band. Furthermore, the band at 1645 cm<sup>-1</sup> for C=C stretching became a shoulder. In the region 2800–3700 cm<sup>-1</sup>, the bands at 2852 cm<sup>-1</sup> for  $\nu_s$ (CH<sub>2</sub>), 2923 cm<sup>-1</sup> for  $\nu_{as}$ (CH<sub>2</sub>), and 3006 cm<sup>-1</sup> for  $\nu_{as}$ (=CH) were very similar. However, the bands for the highly oriented ribbons at 3413 cm<sup>-1</sup> (sharp) and 3330 cm<sup>-1</sup> (shoulder) for  $\nu$ (OH) in the highly oriented ribbons are partially resolved, while only one very broad band at 3420 cm<sup>-1</sup> is observed for the micellar particles.

**Water-Soluble Micellar Dispersions at Neutralized pH Values.** When the SL-COOH aqueous solution was neutralized with sodium hydroxide, the self-association of the corresponding sodium carboxylate SL molecules (SL-COONa) produced water-soluble micellar aggregates. Figure 9A shows the concentration dependence of the apparent  $R_h$  distributions of SL-COONa micellar aggregates at pH = 7.8 determined at  $\theta = 15^\circ$ . At a concentration of 0.02 mg/mL, small aggregates of  $R_h = 37$  nm were formed. When the SL-COONa concentration was gradually increased, the size and size distribution of the micellar aggregates increased and narrowed, respectively. At concentrations from 0.97 to 1.78 mg/mL, nearly monodisperse micellar aggregates were formed with an  $R_h$  of about 100 nm. That is, comparison of the  $R_h$  and dispersity of the micellar aggregates formed at SL-COONa concentrations of 0.97, 1.40, and 1.78 mg/mL shows that the size and size distribution of the micellar aggregates do not significantly change. Thus, the micelles grew with addition of SL-COONa molecules until the  $R_h$

(46) Tandon, P.; Raudenkolb, S.; Neubert, R. H. H.; Rettig, W.; Wartewig, S. *Chem. Phys. Lipids* **2001**, *109*, 37–45.

reached  $\sim 100$  nm. Apparently, some constraint(s) does not allow further expansion of the micelles above 100 nm.

To ascertain the morphology of the micellar aggregates, the angular dependence of  $R_h$  distributions was determined at 1.40 mg/mL and pH 7.8 (Figure 9B). At  $\theta = 15^\circ$ , there exists only a single peak for narrowly distributed micellar aggregates with  $R_h$  of 100 nm. With an increase in the scattering angle, the first peak for the micellar aggregates gradually shifted to smaller apparent  $R_h$  and the  $R_h$  distribution became broader. This is understandable because at higher scattering angles, the observation length scale ( $1/q$ ) is much shorter than the radius of gyration ( $R_g$ ) of the large micellar aggregates. It is impossible to determine the  $R_g$  of the micellar aggregates due to the concentration dependence of the size of the micellar aggregates. Nevertheless, the angular dependence of the scattering intensity of the micellar aggregates at low-angle range ( $15\text{--}35^\circ$ ) allowed us to estimate the apparent  $R_g$  for the large micelles formed at 1.40 mg/mL and pH 7.8, which produced  $R_g$  of 175 nm and a  $R_g/R_h$  value of 1.75. At  $\theta \geq 60^\circ$ , a second peak with an  $R_h$  of about 2.5 nm appeared. Although the peak position of this small peak is independent of the scattering angle, the scattering intensity contributed from the second peak increases with a further increase in scattering angle. We speculate that this second small peak might be related to the internal motion of the micellar aggregates due to the strong intermolecular interactions or the fast mode from the coupled diffusion of the micellar aggregates with counterions. Clearly, this strong angular dependence of the size and size distribution of the micellar aggregates plus the large  $R_g/R_h$  value for the aggregates indicate that the large micellar aggregates have a very anisotropic geometry.

### Conclusion

Sophorolipid molecules displayed intriguing self-assembling behavior. This is due to their unique structural features that include highly asymmetrical polar heads, kinked hydrophobic cores of *cis*-9-octadecenoic chains, and non-amide polar–nonpolar linkages. In acidic conditions

(pH < 5.5), SL–COOH molecules self-organize to form giant twisted or helical ribbons of 5–11  $\mu\text{m}$  wide and several hundred micrometers long. Increasing the pH of SL aqueous solutions decreases the yields of the solidlike ribbon products, slows the formation of giant ribbons, and increases the helicity of ribbons and the inter-ribbon entanglements. The giant ribbons are produced from interdigitated lamellar packing of SL–COOH molecules. The close packing of the kinked hydrophobic *cis*-9-octadecenoic chains and strong disaccharide–disaccharide hydrogen bonding enabled the layered structure to extend to form large highly crystalline ribbons. Neutralizing solutions of SL–COOH with dilute NaOH to pH  $\geq 5.9$  produces clear solutions with short-range ordered micelles. The self-assembly of SL–COONa molecules strongly depends on the solution concentration. At dilute concentrations (<1.0 mg/mL), the size of the micellar aggregates increases with increasing concentration. When the concentration of SL–COONa is above 1.0 mg/mL, narrowly distributed large micellar aggregates with a constant  $R_h$  of 100 nm are formed. The large  $R_g/R_h$  ratio and the strong angular dependence of the size and size distribution of the large micellar aggregates implicate that the large micellar aggregates self-assembled from SL–COONa molecules have an anisotropic geometry.

**Acknowledgment.** S.Z. gratefully acknowledges the support from the National Science Foundation (CHM 0316078) and the CUNY-CSI start-up grant. S.Z. thanks Dr. Igor Scis for his help with the SAXS/WAXS experimental setup at the National Synchrotron Light Source at Brookhaven National Laboratory. Fruitful discussions with Professor Hyuk Yu, Professor Eric Kaler, and Dr. Christian Burger on the structural model of the self-assembled ribbons are greatly acknowledged. R.G., W.G., R.A., and V.S. are all grateful to the members of the NSF Industrial-University Cooperative Research Center for Biocatalysis and Bioprocessing of Macromolecules at the Polytechnic University for their financial support during the performance of this research.

LA048590S